THE ASTROPHYSICAL JOURNAL, 387:551–560, 1992 March 10

LINE FLUORESCENCE FROM THE RING AROUND SUPERNOVA 1987A

ELI DWEK[1] AND JAMES E. FELTEN[1,2]
Infrared Astrophysics Branch, Laboratory for Astronomy and Solar Physics, NASA Goddard Space Flight Center
Received 1991 May 28; accepted 1991 September 11

ABSTRACT

We review observations in λ5007 which reveal an ellipse of line emission around SN 1987A. Spectroscopy suggests that it is an inclined ring of gas, presumably excited by the UV flash associated with shock breakout. The occurrence of this flash was confirmed earlier by *IUE* observations of narrow fluorescent lines from the SN. We derive a simple expression for the rate at which the kinematically accessible paraboloid sweeps over the length of a thin uniform circular ring, and present a simple integral expression for the light curve $F(t)$ of a fluorescent line in terms of $\epsilon(t)$, the local line emissivity. Our resulting light curves agree well with computations by Lundqvist but not so well with those by Panagia and Gilmozzi. This, together with the variety of possible light curves and the uncertainties in the ring geometry and morphology, suggests that the claimed error bar ($\pm 6\%$) on the distance determination by Panagia et al. should be treated with caution.

We graph many simple examples of the relationship between $\epsilon(t)$ and $F(t)$ and use the results to deduce the characteristics of the local emissivity functions which will produce the best fit to the observed N III] λ1750 and N V λ1240 light curves. Adopting physical models by Lundqvist and Fransson for an optically thin gas, in which the functions $\epsilon(t)$ for these lines peak only after recombination has occurred, we find poor agreement with the observed light curves for these lines. Better agreement is obtained if $\epsilon(t)$ responds quickly to the UV flash and persists $\sim$300 days afterwards (suggesting that the ring may have been optically thick to the UV flash); a characteristic arcsine shape is then seen on the leading side of the light curve. The different shape of the N IV] λ1485 light curve remains a puzzle.

We invert the N III and N V light curves to find the functions $\epsilon(t)$ which give best fits to the observations. The inversions are affected by scatter in the data. Nevertheless they give marginal evidence that an additional gas cloud is contributing to the UV line fluxes at $t \gtrsim 700$ days.

Subject headings: galaxies: distances — galaxies: Magellanic Clouds — stars: circumstellar shells — stars: individual (SN 1987A) — stars: supernovae

1. INTRODUCTION

On 1990 August 23–24, the *Hubble Space Telescope* (*HST*), observing in [O III] λ5007, detected an elliptical ring of emission on the plane of the sky, centered on Supernova 1987A, with a major axis $\approx 1''.66$, corresponding to 1.31 lt-yr at 50 kpc (Jakobsen et al. 1991; Panagia & Gilmozzi 1991). This ring had been noted earlier in observations at lower resolution (Wampler et al. 1990; Crotts, Kunkel, & McCarthy 1989). The new high-resolution photograph prompts a reappraisal (Felten & Dwek 1991a; Lundqvist 1991) of theoretical work by Lundqvist & Fransson (1991, hereafter LF; cf. Fransson & Lundqvist 1989). They had some success in modelling the ultraviolet line fluxes from the supernova, detected by the *International Ultraviolet Explorer* (*IUE*) (Fransson et al. 1989) for some hundreds of days following the explosion, as reradiation from a spherically symmetric shell with radius ≈ 0.5 lt-yr, excited by the UV burst. They also predicted optical line fluxes from the same shell. Presumably the hypothetical shell in this work by LF is to be identified with, or is related in some way to, the observed ring.

One might suppose that the elliptical ring is simply a limb-brightened ellipsoidal shell, not very different from the LF spherical shell. The *HST* observers (Jakobsen et al. 1991; Panagia et al. 1991) reject this, suggesting that the surface-brightness contrast between the dark interior of the ring and its bright edge is too great to agree with a limb-brightened model. They assume that the observed elliptical ring is really a circular ring of fluorescing gas centered on the SN, with axes appearing unequal because of the inclination angle. The axial ratio is $(1''.66)/(1''.21)$, which gives an inclination $i \approx 43°$. The semi-major axis, (1.31)/2 lt-yr or 239 lt-days, is the radius R of the ring. (We assume a distance $D = 50$ kpc throughout.)

In this paper, we first discuss in § 2 the general kinematics. We point out that utter dismissal of an ellipsoidal-shell model may be premature, because the kinematical properties of a fluorescent light echo, having a local emissivity function $\epsilon(t)$ of unknown functional form, with nonzero spread in time and responding to the transient SN source, make the calculation of the expected center-to-edge contrast a nontrivial problem. There is, however, additional (spectroscopic) evidence favoring a ring geometry (Wood & Faulkner 1989; Crotts 1991; Crotts & Heathcote 1991; Meikle et al. 1991). Therefore we turn to a ring model.

The computations by LF could be repeated for a ring of gas centered on the SN. This has recently been done in part by Lundqvist (1991). Indeed, agreement with the observed light curves of the *IUE* lines is improved in a ring model by suitable choices of parameters. It is useful to have some analytical results to check these computations, to cast light on general features of the results for a ring, and to assist in visualizing a wide range of possible cases. Therefore we develop the geometry and kinematics of a thin-ring model in § 3, presenting an analytical solution for the motions in three-dimensional

[1] Postal address: Code 685, Goddard Space Flight Center, Greenbelt, MD 20771.
[2] Also Universities Space Research Association.

space of the contact points between the thin ring and the leading kinematically accessible paraboloid. From this we obtain in § 4.1 a simple integral expression for the light curve of a fluorescent echo from a thin uniform ring. We calculate the light curves $F(t)$ which may be observed in a line emitted by the ring, for different possible choices of the time behavior for the local line emissivity, $\epsilon(t)$. Our results agree well with computations by Lundqvist (1991), but not with the theoretical light curves of Panagia & Gilmozzi (1991).

In § 4.2 we calculate possible light curves for the UV lines N III] λ1750 and N V λ1240 and compare them with data. For local emissivity functions in the lines, we first adapt computed physical results from the LF model, using analytical approximations to their curves, but, finding bad agreement, we then explore other forms which give better agreement with the line data. In § 5 we reverse the process, inverting the observed light curves for these same lines to determine the emissivity functions which would give *best* agreement. Finally, in § 6, we discuss physical reasons for departures of the best-fit emissivity functions from the earlier theory, and we add some remarks on other aspects of the observations.

Continued fluorescence in [O III] λ5007 at present, more than 1300 days after core collapse, must be reduced from its earlier peak if the high-density models of LF are applicable. Study of the observed line fluxes for several late epochs will eventually test this. A neighboring lower-density envelope could produce higher fluxes in this line at late times.

2. KINEMATICS AND THE SHELL MODEL

Reradiation by a shell or ring shares many features with the classical problem of light echoes by reflection (Couderc 1939; Morrison & Sartori 1969; Bahcall, Kozlovsky, & Salpeter 1972; Wright 1980; Blandford & McKee 1982; Dwek 1983; Emmering & Chevalier 1988; Felten, Dwek, & Viegas-Aldrovandi 1989). The line excitation is due almost entirely to the UV burst at day 0 (core collapse). The region kinematically accessible to observation at a time t days later is bounded by a "leading paraboloid." If the shell or ring has radius, say, $R = 0.5$ lt-yr, then it lies entirely within the paraboloid at $t = 2R/c = 365$ days, and farther within at all subsequent times. Because the reradiation in a particular line is not instantaneous but has a local emissivity curve which takes time to rise and fall, the entire region within the paraboloid is in principle observable at time t.

At late times (1990 August 23 = day 1277), all portions of the shell are observed long after their initial excitations. For a spherical shell, the delay (difference between the actual time of observation and the time of entry into the paraboloid) is greatest for the front point and least for the back point (which are superposed in projection at the center), and it is intermediate for the points seen on the limb. Prediction of the surface-brightness profile involves knowledge of the emissivity curve (possibly position-dependent) for the line in question, and no such prediction is obtainable immediately for comparison with profiles observed by Jakobsen et al. (1991).

The computations of LF could be extended to predict this profile in λ5007 for a spherical shell, and could be generalized to an ellipsoidal shell. Until this has been done, the shell model should not be dismissed completely. We note, however, that in the high-density ($n_e \gtrsim 10^4$ cm^{-3}) models favored by LF to fit the *IUE* data, the λ5007 local emissivity peaks at $\approx$200 days delay and falls off by $\approx$400 days, so that at day 1277 the fluxes received from all elements on the shell, being all delayed by $\sim$(1277–365) days or more, should be very much reduced from their earlier peaks. This may not be inconsistent with the observations, but it shows that study of the late tail of the emissivity curve will be necessary to predict the surface-brightness profile and test the model. Only a long ellipsoid or an elliptical cylinder, with long axis nearly along the line of sight, could approach the leading paraboloid and sample earlier parts of the emissivity curve at day 1277.

It is of interest that the controversy of rings versus shells has a long history with respect to the simpler case of *non*-transient nebulae (planetaries). Curtis (1918) claimed that the Ring Nebula must be a true ring rather than a shell, using essentially the same argument as Jakobsen et al. (1991). For the Ring Nebula and other planetaries, the controversy continues (Minkowski & Osterbrock 1960; Atherton et al. 1978; Reay & Worswick 1979; Balick & Preston 1987).

3. A RING MODEL

Spectroscopic observations (Wood & Faulkner 1989; Crotts 1991; Crotts & Heathcote 1991; Meikle et al. 1991) show that the ellipse of emission on the plane of the sky has a radial-velocity gradient roughly parallel to its minor axis, i.e., little or no gradient along its major axis. This is the velocity signature of a radially expanding (or contracting) ring, tilted about the major axis, rather than a limb-brightened shell. The major axis has position angle 80° ± 5°, according to Jakobsen et al. (1991); i.e., it is roughly east-west. [The value of this P.A. is not important in our calculations. Parenthetically we note, however, that there is disagreement about it, by up to 20°, in the literature (Crotts & Heathcote 1991; see Wampler et al. 1990). We are not sure that all published images are aligned correctly. They should be compared with the astrometry of the field (e.g., Walborn et al. 1987; Heap & Lindler 1987; Girard, van Altena, & Lopez 1988; Testor 1988; Paresce & Burrows 1989; Walker & Suntzeff 1990.]

The velocity gradient is positive toward the south. With the reasonable assumption that the ring is expanding from the progenitor star rather than contracting, the observers conclude that the north point of the ring (roughly speaking) is closest to us and the south point is farthest away. The radial expansion velocity implied for an inclination of 43° is 10–15 km s^{-1}.

Noting this strong evidence in favor of a ring, we turn to obtaining some simple results for a circular ring model, which we assume to be ideally thin, with cross-sectional dimensions $\ll R$, and centered on the SN. This leads to simple analytical results. These results, of course, will not apply exactly to more elaborate ring models used in computations, e.g.: (1) a right circular cylinder with small but nonzero height $h < R$ and negligible radial thickness $\Delta R \ll R$, centered on the SN; (2) a narrow equatorial belt on a sphere centered on the SN, confined to a latitudinal band $|b| \leq \theta/2$, with negligible radial thickness $\Delta R \ll R$ (Lundqvist 1991; Panagia & Gilmozzi 1991; N. Panagia 1991, private communication); or, more generally, (3) a fat torus with arbitrary toroidal cross section. Computational results for all such models should, however, approach ours in the limit when the largest cross-sectional dimension is $\ll R$. Our model is therefore useful as a check on computations.

We use right-handed xyz coordinates, with the SN at the origin, x and y in the plane of the sky, and positive z toward the observer. The normal to the ring plane makes inclination angle $0 \leq i \leq 90°$ with the positive z-axis. We choose the positive x-axis in the direction of this inclination; i.e., the point on the ring farthest from the observer projects, on the plane of the sky,

onto the positive x-axis. (For the observed ring, the position angle of positive x is nearly south.) The ring is then the intersection of a plane and an elliptical cylinder:

$$z = -x \tan i ; \tag{1}$$

$$R^2 = \frac{x^2}{\cos^2 i} + y^2 . \tag{2}$$

The leading paraboloid at observation time t after core collapse is given by

$$z = \tfrac{1}{2}ct[(r/ct)^2 - 1] , \tag{3}$$

where $r^2 \equiv x^2 + y^2$ (Couderc 1939; Morrison & Sartori 1969; Wright 1980). Combining equations (1)–(3) gives the positions of the points (x, y, z) where the ring and paraboloid intersect at time t, as functions of t. Using the fact that $|x| \leq R \cos i$ to resolve a sign ambiguity, we solve and find

$$x = (ct - R) \cot i ; \tag{4}$$

$$y^2 = R^2\left[1 - \left(\frac{ct}{R} - 1\right)^2 \csc^2 i\right]; \tag{5}$$

$$z = R - ct . \tag{6}$$

The contact point initially appears on the ring with $y = 0$, $x = -R \cos i$, and $z = R \sin i$, at time t_i given by

$$t_i = R(1 - \sin i)/c . \tag{7}$$

On the plane of the sky, this point projects onto the negative x-axis and is close to the north point on the ring. It splits into two points (as indicated by the y^2 in equation [5]), which travel around opposite sides of the ring, finally merge, and disappear from the ring on the positive x-axis (in projection) at time

$$t_f = R(1 + \sin i)/c . \tag{8}$$

Equation (6) says that the z coordinate of the contact points decreases at constant rate c—an interesting result which was not obvious. Equations (4) and (5) describe the projected motions of the contact points on the plane of the sky.

Differentiating equations (4) and (5) to form the element $ds^2 \equiv dx^2 + dy^2$, we find the apparent speed of motion of each contact point on the plane of the sky:

$$\frac{ds}{dt} = c\left\{\frac{\cos^2 i + [(ct/R) - 1]^2}{\sin^2 i - [(ct/R) - 1]^2}\right\}^{1/2} . \tag{9}$$

Note that if $i < 45°$ ($\cos i > \sin i$), the speed is continuously superluminal from the time of initial contact t_i to the time of final contact t_f. It is infinite at t_i and t_f, when the paraboloid and ring are tangent. If $i > 45°$, the speed is subluminal for $t \approx R/c$, but it still approaches infinity near t_i and t_f.

A historical sidelight (Felten 1991): Hinks (1902), discussing the rapidly moving nebulosities around Nova Persei 1901, understood this possibility of superluminal motion and sketched correctly the motions of the projected contact points on an inclined ring for the case $i = 60°$, $R = 3.73$ lt-yr. Possibly intimidated by Kapteyn's (1901) alternative explanation (which ostensibly did not involve superluminal motion), Hinks (1902) failed to follow up on this. Consequently the superluminal character of the motions around Nova Persei 1901 (which in fact were not on a ring but on foreground clouds) was not appreciated until Couderc (1939).

Differentiating equation (6) and combining with equation (9) to form the element $dl^2 \equiv dx^2 + dy^2 + dz^2$, we find a simple expression for the element of length along the ring which the paraboloid sweeps over in time dt (Felten & Dwek 1991a):

$$dl = 2c\,dt\{\sin^2 i - [(ct/R) - 1]^2\}^{-1/2} \tag{10}$$

for $t_i < t < t_f$, and zero otherwise. The factor 2 appears because there are two contact points. An easy but powerful check of equation (10) may be done by noting that, between t_i and t_f, the integral of dl is $2\pi R$. The function dl/dt and its integral $l(t)$ (the length of ring within the paraboloid at time t) are shown in Figure 1. Note that dl/dt is formally infinite at t_i and t_f. The integral $l(t)$ is an arcsine function (see § 4.1) and remains finite.

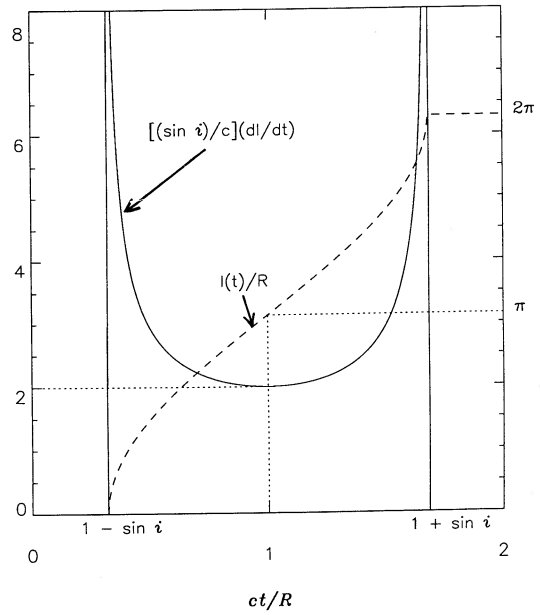

FIG. 1.—*Solid curve*: the instantaneous rate dl/dt at which the leading kinematically accessible paraboloid sweeps over the length of a thin ring (centered on the supernova, with radius R and inclination angle i), shown as a function of time t after the SN core collapse is seen. The two peaks are formally infinite and occur when the paraboloid is tangent to the ring. Quantities plotted are chosen so that the axes are dimensionless. The graph is prepared for $i = 43°$ ($\sin i = 0.682$). *Dashed curve*: the integral of dl/dt; i.e., the length of ring within the paraboloid at time t.

[In contrast, for a symmetric spherical shell, the rate at which *area* on the shell is swept into the paraboloid is constant from time $t = 0$ to time $t = 2R/c$, when the paraboloid leaves the shell. This result became apparent in applications (Morrison & Sartori 1969; Bahcall et al. 1972; Wright 1980; Blandford & McKee 1982; Dwek 1983; Chevalier 1986) and is now familiar (Fransson et al. 1989).]

4. LIGHT CURVES FOR *IUE* LINES

4.1. *Possible Light Curves*

The *IUE* data, lacking sufficient angular resolution, cannot show us the motions of the contact points. We must consider instead the total fluxes received in the individual lines. The "observed line luminosity" from the ring, $L(t)$, is defined (Lundqvist & Fransson 1991) by the light curve for the flux in a given line, $F(t)$, and these quantities are given by

$$L(t) \equiv 4\pi D^2 F(t) = \int_0^t dm(t')\epsilon(t - t') , \tag{11}$$

where D is the distance, $\epsilon(t)$ is the local emissivity function in

this line (in units of ergs s^{-1} g^{-1}) at time interval t after local excitation by the UV signal from core collapse, and $dm(t) = \rho A\, dl(t)$ is the mass element along the ring, assumed to have a uniform mass density ρ and cross-sectional area A, with dl given by equation (10).

All of the atomic physics of the problem is contained in the local emissivity function $\epsilon(t)$. For a given line, its time behavior depends on the intensity, spectrum, and duration of the UV burst, and the number density of the atomic species. The function rises "instantaneously" if the ionization state of the emitting species is a "primary" one created by the UV burst, and rises more slowly if it is "secondary"—a result of recombination from a higher ionization state. The subsequent behavior of the line is determined by the combined effects of recombination and cooling in the ring material. Computed emissivity curves for a variety of lines and two types of bursts are given in Figure 2 of LF. Equation (11) assumes that $\epsilon(t)$ is the same at all points along the length of the ring. This must be true by symmetry if the ring is circular and uniform and the UV burst is spherically symmetric. We have neglected any dependence of $\epsilon(t)$ on position within the thin ring: for example, on radial distance R from the SN along a path through the ring. This would be incorrect under some circumstances: for example, if the ring material were optically thick to the UV burst (Lundqvist 1991). In such cases equation (11) could still be used if $\epsilon(t)$ were interpreted as a mean over the mass in the ring.

For purposes of illustration, we will present the evolution of $F(t)$ for several "generic" emissivity functions $\epsilon(t)$: (case a) a delta function $\delta(t-\tau)$, representing instantaneous rise and decline of the emission. Primary lines emitted from high-density regions and dust reflections of the UV burst are characterized by such a function, with $\tau = 0$. The case $\tau > 0$ is unphysical but makes a useful illustration. (case b) A function rising abruptly at $t = 0$ and remaining constant after $t = 0$, characteristic of emission by a species for which recombination and cooling can be neglected. (case c) A function which is zero for $t < 0$, but for $t > 0$ is a Gaussian with peak at $t = \tau$ and standard deviation σ. For small or zero τ this function characterizes a primary ion with a nonzero recombination time, such as O VI in the figures of LF. (case d) A function rising exponentially from zero to some time τ, after which it decreases as a Gaussian. This function was chosen to characterize the behavior of a secondary ion such as N III. The following equation summarizes the various functional forms of the emissivity function for $t \geq 0$:

$$\frac{\epsilon(t)}{\epsilon_0} = \delta(t-\tau) \qquad \text{case a} \qquad (12a)$$

$$= 1 \text{ (constant)} \qquad \text{case b} \qquad (12b)$$

$$= \exp\left[-\frac{(t-\tau)^2}{2\sigma^2}\right] \qquad \text{case c} \qquad (12c)$$

$$= 0.632121\left[1 - \exp\left(\frac{-t}{\tau}\right)\right] \qquad \text{case d} \quad t < \tau$$

$$= \exp\left[-\frac{(t-\tau)^2}{2\sigma^2}\right] \qquad \text{case d} \quad t > \tau\,. \qquad (12d)$$

The normalization constant ϵ_0 denotes the peak value in the latter three cases. Various examples of these functional forms are shown in the left-hand panels of Figure 2, normalized arbitrarily.

Figure 2 depicts also the light curves $F(t)$ for various choices of the functions described above. For each case, the chosen emissivity function is shown on the left and the resulting light curve $F(t)$ on the right. All calculations were performed for a ring of radius $R = 239$ lt-days, and an inclination of 43° ($\sin i = 0.682$), for which the times of first and last contact between ring and leading paraboloid are $t_i = 76$ days and $t_f = 402$ days. Normalizations in all these panels are arbitrary, and the vertical dashed lines on the right show t_i and t_f. Figure 2*a* illustrates schematically a delta function (eq. [12a]) at $\tau = 0$ days. The resulting light curve (Fig. 2*a'*) is the behavior expected for an instantaneous reradiation or an echo reflection. It is essentially the same as the double-peaked curve dl/dt in Figure 1. In Figure 2*b*, we replace the delta function by a Gaussian peaked at the origin, with a fairly rapid falloff $\sigma = 50$ days. Figures 2*c* and 2*d* increase σ to 100 and then 200 days. Figure 2*e* illustrates the constant emissivity function with onset at $t = 0$ (eq. [12b]), In this case $F(t)$ (Fig. 2*e'*) is essentially the integral of equation (10), i.e., the curve l/R in Figure 1, and is an arcsine function (Felten & Dwek 1991a):

$$4\pi D^2 F(t) = 0 \qquad t < \frac{R}{c}(1 - \sin i)$$

$$= \pi^{-1} M_R \epsilon_0 \left\{\arcsin\left[\frac{(ct/R) - 1}{\sin i}\right] + \frac{\pi}{2}\right\} \qquad (13)$$

$$\frac{R}{c}(1 - \sin i) < t < \frac{R}{c}(1 + \sin i)$$

$$= M_R \epsilon_0 \qquad t > \frac{R}{c}(1 + \sin i)\,,$$

where M_R is the ring mass. Figure 2*e'* shows the arcsine behavior of the light curve for $Rc^{-1}(1 - \sin i) < t < Rc^{-1}(1 + \sin i)$.

Figures 2*b*–2*d* illustrate practical cases (primary lines with fast or slow falloff) which approach the ideal cases 2*a* and 2*e* as limits. The resulting light curves mimic either the two-peaked (derivative of arcsine) behavior characteristic of the delta function, or the arcsine behavior produced by constant emissivity, depending on whether the falloff is fast or slow.

Figure 2*f* shows a delta function at $\tau = 45$ days. This unphysical case illustrates that the double-peaked light curve is simply displaced to the right by 45 days. Figures 2*g*–2*i* assume exponential Gaussians (eq. [12d]) with $\tau = 45$ days and $\sigma = 50$, 80, 200 days. These light curves would correspond to "secondary" lines which appear and rise to a peak soon ($\sim$45 days) after the UV burst and die away rapidly or slowly. The light curves are displaced to the right, compared to the previous set, because of the nonzero τ. Note that the peak of the light curve is displaced from t_f by $\sim$30 days. The light curves once again approach the two-peaked or the arcsine behavior in the limit of short or long σ. Lundqvist (1991) describes some of his computed curves (for N V λ1240 in his Fig. 1) as "arcsine" curves. The light curve for this line in his Figure 1*b* resembles closely our Figure 2*h'* above. This is good, because we chose the particular parameters of Figure 2*h* with the intention of checking Lundqvist's results (see also § 6). These curves are actually closer to the two-peaked case than to the arcsine case.

Figure 2*j* shows a delta function at $\tau = 200$ days. Figure 2*k* is a Gaussian with $\tau = 200$ days and $\sigma = 50$ days. Figures 2*l*–2*n* are exponential Gaussians (eq. [12d]) with $\tau = 200$ days and $\sigma = 50$, 100, 200 days. This sequence shows a variety of two-humped behavior, and it shows that the peak of the light curve

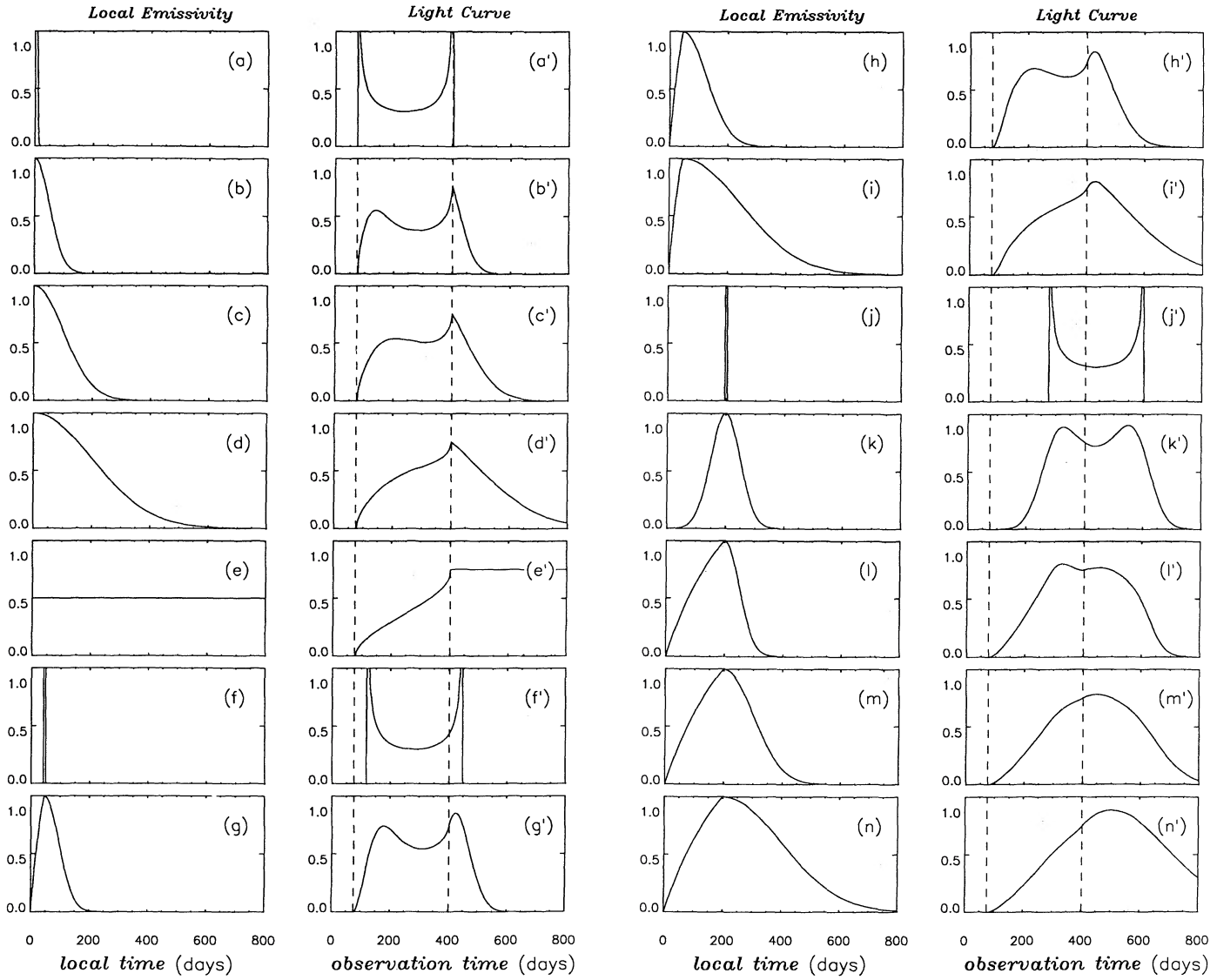

FIG. 2.—14 examples, computed from eq. (11), of the relationship between (a–n) the local emissivity function in a line, $\epsilon(t)$, and (a'–n') the received light curve $F(t)$ in that line for a thin uniform ring. We assume $R = 239$ light days and $i = 43°$. In each case, the assumed form of $\epsilon(t)$ is shown on the left and the resulting $F(t)$ on the right. The local emissivity functons in this and other figures are plotted versus *local* time, measured since the local excitation by the UV burst, whereas light curves are plotted vs. *observation* time, measured since core collapse. Normalizations are all arbitrary. Functional forms and specific values of parameters for the functions $\epsilon(t)$ assumed are given in the text.

can be displaced from t_f *in either direction* by a large amount. It also shows that the arcsine behavior on the front side of the light curve is lost when the rise on the front side of $\epsilon(t)$ is slow.

The collected results in Figure 2 show that a wide range of behavior in the light curve is possible, depending on the assumed emissivity function $\epsilon(t)$. The calculated light curves of Panagia & Gilmozzi (1991) do not resemble any of those in Figure 2. They used a two-component model, and we await publication of further details. However, the mass accretion rate used in their calculations is not compatible with our equations (10) and (11) (N. Panagia 1991, private communication). We believe that the results from their analytic geometry are not applicable to a uniform-ring model.

4.2. *Calculations for Comparison with Data*

Recently Panagia et al. (1991) have used the *IUE* light-curve data to derive a distance D to the supernova: 51.2 ± 3.1 kpc. We note that the model light curves of Panagia & Gilmozzi (1991), which appear to be incorrect, were used in fitting the data. We also note that the method used assumes that the light curve of each line peaks at the time of final contact t_f. Our collected results in Figure 2 show that this assumption may be too restrictive. In view of the many uncertainties concerning the geometry of the ring and the emissivity functions, we feel that the claimed error bar on the distance is optimistic (Felten & Dwek 1991b). We defer further discussion of this to a later paper.

To compare theory with the observed light curves in the lines, we have to make a choice of $\epsilon(t)$, preferably on physical grounds. For a first try, we can take physical (theoretical) results of LF for a spherical-shell model and adapt them for use on a ring. The Lundqvist & Fransson (1991) Model M1 has radius 0.5 lt-yr, density $\rho = 5.1 \times 10^{-20}$ g cm^{-3} with cosmic abundances, and a total mass $M = 0.025\ M_\odot$. Its maximum electron density (after the UV burst) is $n_e = 2.6 \times 10^4$ cm^{-3}. We can take this mass from the shell and put it all on the thin

ring instead, *keeping the same* ρ, which controls the time behavior of $\epsilon(t)$. (The layer will have to be much thicker then.) The ring is 0.65 lt-yr from the SN rather than 0.5, but this will matter little to $\epsilon(t)$ provided the model remains *optically* thin to the UV burst. Concentrating first on the line N III] λ1750, we obtain an analytical approximation to $\epsilon(t)$ as follows: We use our functional form (12d) above (N III is a secondary ion), normalizing to the computed $\epsilon(t)$ of LF (their Fig. 2*a*, middle panel) at the peak ($M_R \epsilon_0 \approx 16 \times 10^{35}$ ergs s^{-1}), and assuming $\tau = 200$ days and $\sigma = 96$ days to give a reasonably good fit to the shape of their curve. It is useful to graph the product $M_R \epsilon(t)$ rather than $\epsilon(t)$ when properly normalized curves are to be drawn, because if D, R, and $dl(t)$ (eq. [10]) are known, the product $M_R \epsilon(t)$ determines the light curve $F(t)$ (including normalization), and vice versa. The quantities M_R and $\epsilon(t)$ need not be known separately, and in general they are not, unless there is a complete physical model as in the LF case.

Our resulting approximate fit to the $M_R \epsilon(t)$ given by LF for λ1750 is shown in Figure 3*a*. We may now compute $F(t)$ from equation (11), using the same D (= 50 kpc) assumed by LF. The resulting light curve is compared with data for this line in Figure 3*b*. For light-curve data, we use the corrected (dereddened) line fluxes published by Fransson et al. (1989) for times prior to day 400. From day 400 to day 1200 we start with *observed* line fluxes given by Sonneborn (1989, and 1991, private communication) and by Sonneborn et al. (1990). For continuity with the earlier data, these late data must be dereddened. The dereddening factor may be inferred from a comparison of the two data sets at day 416. This factor is 5.6 at λ1750 and 10.8 at λ1240.

We are not yet able to evaluate the goodness of fit quantitatively, because the standard errors of the *IUE* data points have not yet been published. However, this expected light curve is clearly not a good fit to the data. The fact that the peak of the curve lies far above the data is not in itself a cause for concern. We are free to renormalize the curve. The normalization by LF, which was done by choosing $M = 0.025\ M_\odot$, was preliminary and approximate. They did not do exact normalizations to data in individual lines, preferring to have factor-of-2 agreement between their shell model M1 and a wide variety of UV and visual lines. In fact our Figure 3*b* is in qualitative agreement with the comparisons for UV lines in their Table 3.

Renormalizing our curve in Figure 3*b* by least-squares, we could find a better fit with $M_R \approx 0.018\ M_\odot$. Keeping the same density, this would correspond to a ring with somewhat smaller cross section A. The curves in Figures 3*a* and 3*b* would then both lie lower by a factor 18/25. This would be, in effect, a redetermination of the mass by the LF method, adapted specifically to a ring model and to the line λ1750. Since the model mass is $2\pi R \rho A$, the cross-sectional area A of the ring would be 1.8×10^{32} cm^2 in this case. Since $A^{1/2} \ll R$, the thin-ring approximation is probably valid. (It would not necessarily be valid if the ring cross section were extremely oblong.)

Even this renormalized curve would not be a great fit to the data. The shape is wrong. But in fact the light curves of LF for the shell model did not fit the line data well either. The ring model has one definite advantage: Unlike the shell model (Fransson & Lundqvist 1989; LF), it predicts zero flux prior to the time in equation (7). This agrees better with the data. It makes sense to assume provisionally that the ring geometry is correct and to ask: What function $M_R \epsilon(t)$ would give a better fit to the light curve? Inspection of Figure 2 leads us quickly to the fits shown in Figure 4*b*. Here we have assumed that $\epsilon(t)$ is of the form of equation (12c) with $\tau = 0$ and $\sigma = 200$, 300, 400 days (shown in Fig. 4*a*); i.e., the UV burst creates a lot of N III immediately, and the line emission of N III in λ1750 decreases with a fairly long time constant. These choices of σ all give passable fits to the decay on the back side of the light curve and are long enough so that the characteristic arcsine shape is seen on the front side and gives a good fit there. Judging by least squares, the fit with $\sigma = 300$ days is preferred. Clearly, however, we could improve the fit further if we were take a smaller σ (200 or 250 days) and assume that the extra flux at $t > 700$ days arises in some other source—possibly another

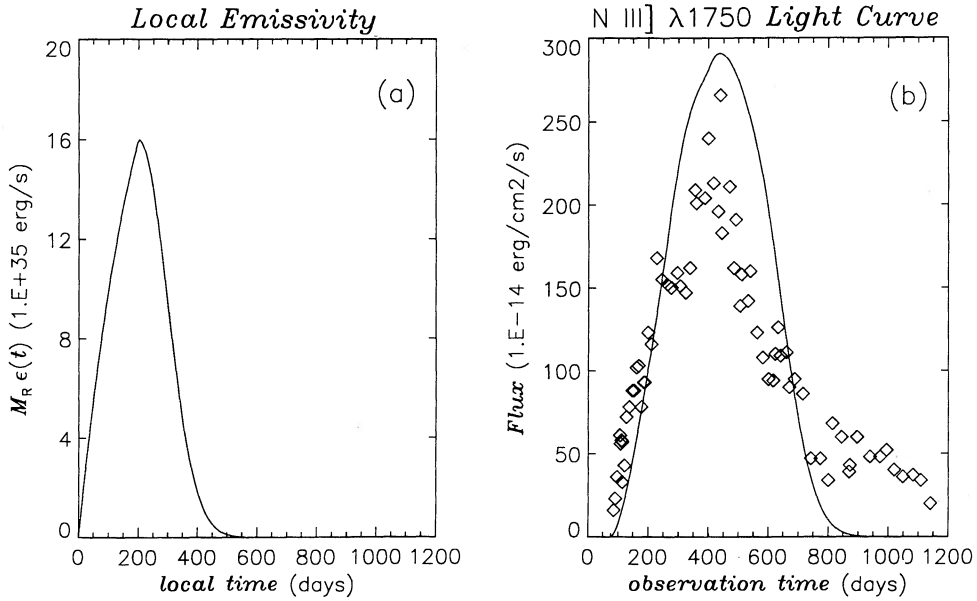

FIG. 3.—(*a*) Analytical approximation to the product $M_R \epsilon(t)$ (ring mass times emissivity) computed by LF for an optically thin cosmic plasma of density 5.1×10^{-20} g cm^{-3} and total mass 0.025 $M_\odot$, for the line N III] λ1750. (*b*) The resulting light curve for this line if the plasma is distributed uniformly on the thin ring, compared with corrected (dereddened) observations. See text. The normalization of the theoretical curve is not mandatory, and it can be lowered. Figures 3–8 assume $R = 239$ light days, $i = 43°$.

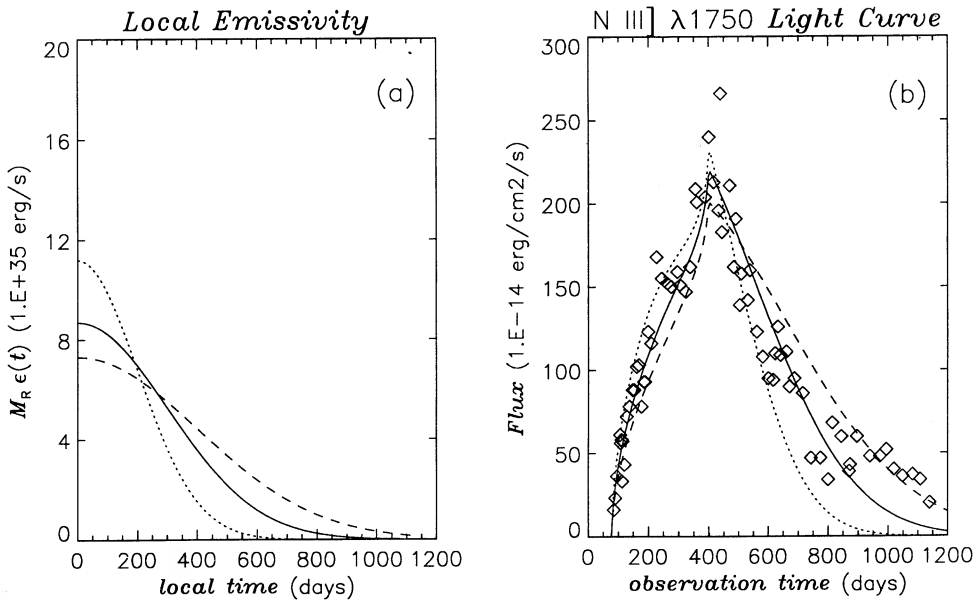

FIG. 4.—(*a*) Assumed functions $M_R \epsilon(t)$ for the line λ1750, of half-Gaussian form, peaked at the origin, with $\sigma = 200$ (*dotted curve*), 300 (*solid curve*), or 400 days (*dashed curve*). (*b*) The light curves produced by these three functions, compared with corrected (dereddened) observations. Normalizations in each case have been chosen to provide least-squares fits in Fig. 4*b*.

cloud or clouds, external to the ring. We return to this possibility in § 5.

We emphasize that this half-Gaussian form of $\epsilon(t)$ for the ring is as yet based on no physical model. Therefore we can determine the normalization of $M_R \epsilon(t)$ by the least-squares fit as shown, but we cannot determine M_R and ϵ separately. The ring mass, however, might well be of the same order as that derived above—a few percent of a solar mass.

We can play the same game with the data for line N v λ1240. The emissivity function computed for this line by LF in their Model M1 is fitted well by our form of equation (12d) with $\tau = 45$ days and $\sigma = 80$ days. The computed light curve for this case already appears in our Figure 2*h*′. (We chose parameters of some of the illustrative cases with this application in mind.) A light curve of this shape cannot provide a good fit to the λ1240 data, which are shown as points in Figure 5*b*. But an emissivity function of the form of equation (12c) with $\tau = 0$ and $\sigma = 350$ days (shown in Fig. 5*a*) produces the light curve shown in Figure 5*b* (normalized by least squares), which is a passable fit. Alternative fits with $\sigma = 250$ and 450 days are also shown. (Once again we might want to consider the possibility of an additional contribution to the flux at $t > 700$ days.) The data are fitted well by emissivity functions for N III] λ1750 and N v λ1240 which are not very different from one another. This

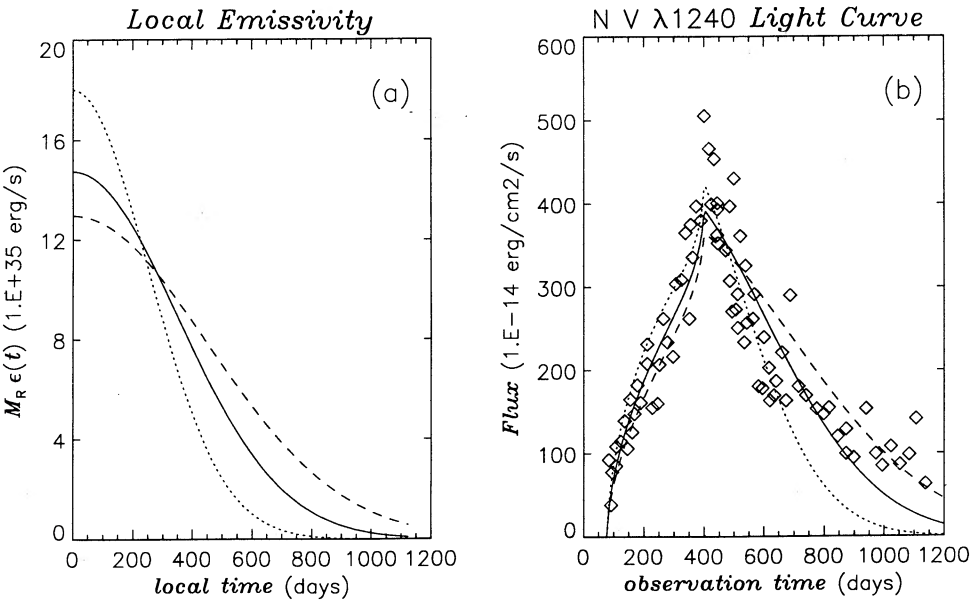

FIG. 5.—Same as Fig. 4, but for the line N v λ1240. The values of σ in this case are 250, 350, 450 days

is not expected in the optically thin models of LF, where N III is much slower to form by recombination than N V. We discuss this further in § 6.

5. INVERSION OF THE LIGHT CURVES

The *IUE* light curves $F(t)$ published so far (Fransson et al. 1989; Sonneborn 1989; Sonneborn et al. 1990) are preliminary, but it is worth while to consider inverting them to indicate what could be learned from high-precision data. If $F(t)$ is not too noisy, the integral equation (11) can in principle be inverted to give the emissivity function $\epsilon(t)$ for a given line. Equation (11) can be transformed into the "faltung" special case of the Volterra equation of the first kind and can be solved for $\epsilon(t)$ by a standard formula (Morse & Feshbach 1953, pp. 992, 995) involving Laplace transforms and complex numbers.

Here we content ourselves instead with doing a simple numerical inversion. Given any functional form $F(t)$ for the light curve in equation (11), we invert $F(t)$ as follows: we replace the integral in equation (11) by a sum over N equal increments ($N \sim 1000$, say), of dt each, between $t_0 \equiv t_i$ and $t_N \equiv t_0 + N\,dt$. Let the grid points be t_k:

$$t_k = t_0 + k\,dt \quad (0 \le k \le N)\,. \tag{14}$$

Let each grid point t_k be taken separately as an upper limit t in equation (11). Then equation (11) generates a set of N equations:

$$\begin{aligned} F_1 &= a_{11}\epsilon_1 \\ F_2 &= a_{21}\epsilon_1 + a_{22}\epsilon_2 \\ &\cdots\cdots \\ &\cdots\cdots \\ F_N &= a_{N1}\epsilon_1 + a_{N2}\epsilon_2 + \cdots + a_{NN}\epsilon_N\,, \end{aligned} \tag{15}$$

where $F_k \equiv F(t_k)$,

$$\epsilon_j \equiv \epsilon\left(\frac{2j-1}{2}\,dt\right), \tag{16}$$

and

$$a_{kj} \equiv \frac{1}{4\pi D^2}\,dm\left(t_k - \frac{2j-1}{2}\,dt\right) = a_{(k+1)(j+1)}\,, \tag{17}$$

so that the a_{kj} are equal along diagonals.

Except for a proportionality constant (mass per unit length), the mass element $dm(t)$ is known for the ring from equation (10). Since the F_k are known from the light curve $F(t)$, equations (15) represent a set of N equations with N unknowns ϵ_j which can in principle be solved by inverting the $N \times N$ matrix a_{kj}. Since half of the matrix ($j > k$) is zeros, the system of equations can be solved more simply by a process of substitution. We note that the first value ϵ_1 is isolated and can readily be calculated, giving $\epsilon_1 = F_1/a_{11}$. This value can then be substituted into the next equation to yield the value of ϵ_2, and so on. The system of N equations given above is thus solved by forward substitution (cf. Press et al. 1986, § 2.2). We use steps of one day each.

To examine the numerical stability of our procedure, we calculated the inverse of an arcsine curve (Fig. 2*e'*), using 800 steps of 1 day each. We know that the exact inverse is a constant (Fig. 2*e*). The numerical inverse, shown as the dotted curve in Figure 6, shows this constant behavior, but also exhibits sharp transients at times $t = 326$ and 652 days, which are multiples of the difference between 402 days and 76 days, the positions of the two peaks in the inversion kernel, dl/dt, shown in Figure 1. The transients arise from the coupling between these two peaks, and contain little net power. Nevertheless the effect of the 326-day transient will be noticeable in all other inversions presented here, in the form of an unphysical *negative* excursion of the emissivity function $\epsilon(t)$. To suppress this transient and other numerical instabilities in the graph, we apply a median filter of width 50 days to the inverse. The result is the solid line in Figure 6.

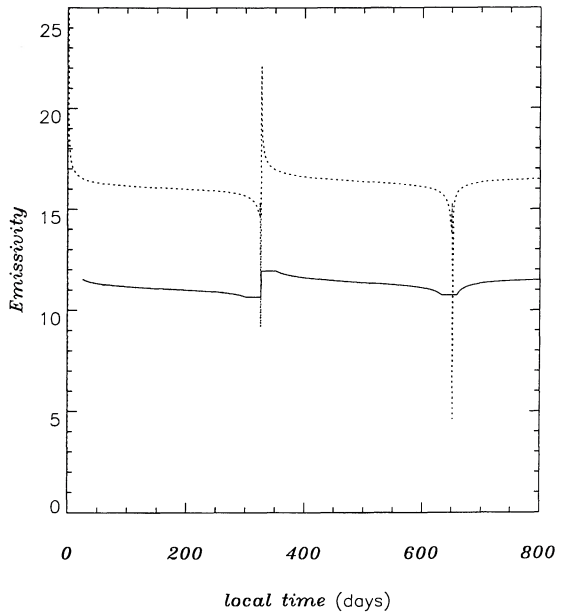

FIG. 6.—Test inversion of an arcsine function (Fig. 2*e'*) by the numerical technique of § 5. Normalizations arbitrary. *Dotted curve*: The direct inverse, using 800 steps of one day each. *Solid curve*: The same output, after a median filter 50 days wide has been applied. The latter curve is offset by 5 units in y, for clarity. The exact inverse would be a constant (Fig. 2*e*).

We now invert the real light-curve data, starting with the N III] λ1750 line. To smooth the data first, we make a least-squares fit of the light-curve data points (Figs. 4*b* and 5*b*) to an nth-degree polynomial $F(t)$, joining the polynomial smoothly to zero at t_i to avoid unphysical results. Figure 7*a* shows the resulting $F(t)$ for $n = 9$. (The characteristic arcsine shape appears when $n \ge 8$, suggesting that this signature of a ring is indeed present in the data.) Figure 7*b* shows the inverse of the $F(t)$ in Figure 7*a*, using 1077 steps of one day each. The inverse shows, as we expect from the earlier fits in Figures 3–4, a rapid rise at zero and persistence over about 300 days. The dip around 100 days need not be taken literally; perhaps data smoothing by a polynomial is not the best scheme. The bumps and negative excursions at $t > 400$ days are unphysical. The reader will see easily that they may be caused by sensitivity of the polynomial fit in Figure 7*a* to noise in the data. On the other hand, they may in some cases indicate shortcomings of the uniform-ring model. For example, as we suggested in § 4, the apparent "tail" on the light curve in Figure 7*a* in the vicinity of 700 to 1100 days could be produced by a separate gas cloud or clouds somewhere near the ring (see Crotts & Heathcote 1991). Then when the light curve is inverted using only the uniform-ring kernel, spurious bumps begin to appear in Figure 7*b* 76 days earlier, i.e., around 600 days. The

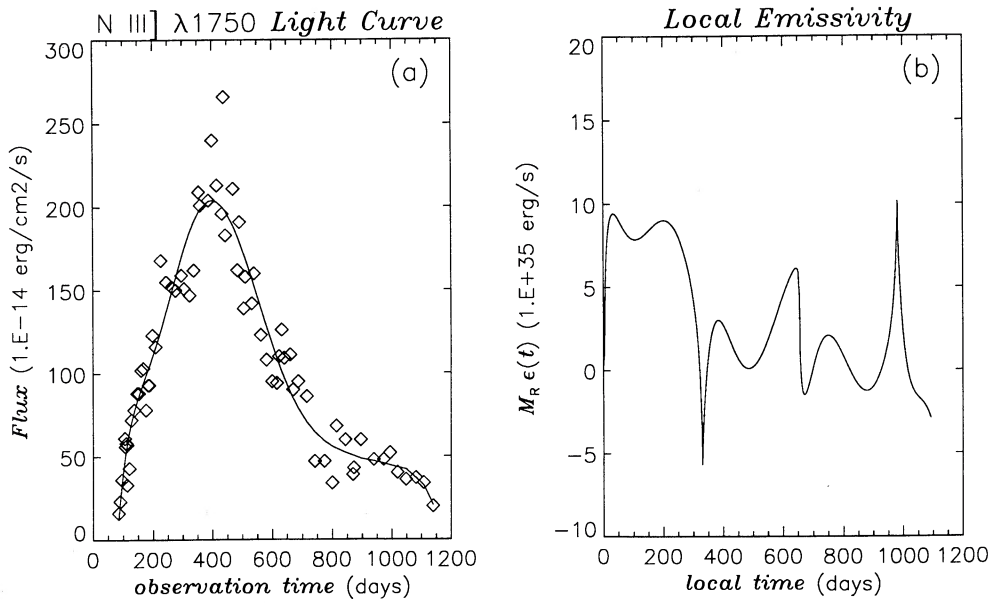

FIG. 7.—Inversion of the observed light curve for the line N III] λ1750. (*a*) We smooth the data by a least-squares fit to a ninth-degree polynomial (*shown*). (*b*) The local emissivity given by the direct inverse of this polynomial using 1077 steps.

unphysical bumps and negative excursions at $t > 600$ days would then indicate that the mass accretion rate in equation (10) does not represent all the gas present, so that the integral in equation (11) needs to be supplemented by another term for an additional cloud. It was already apparent from Figures 4*b* and 5*b* that the fits to the data could be improved by assuming an additional cloud contributing to the observed flux around day 700.

Figures 8*a* and 8*b* show an inversion of the light curve for N V λ1240 by the same technique. The features visible in Figure 8*b* at $t < 800$ days are much the same as in Figure 7*b*. Once again the polynomial fit gives suggestive evidence of a second component in the light curve at around 700 to 900 days, which generates unphysical peaks in the emissivity (Fig. 8*b*) around 600 to 800 days. The dip in the polynomial fit of Figure 8*a* around 1000 days generates a large and unphysical negative emissivity around 900 days. This latter feature is clearly sensitive to noise in the data. While these inversions are interesting, we feel that, in the present state of the data, model fitting as in Figures 3–5, guided by Figure 2, is likely to give quicker insight than numerical inversion as in Figures 6–8.

6. DISCUSSION

Can we see any reason why the emissivity functions $\epsilon(t)$ computed by LF might not be valid when the matter is placed on a ring? The total mass on the shell in LF Model M1 is 0.025 $M_\odot$. For comparison, the total mass which *could have been ionized* by their model UV burst (spread over 4π sr) was ~ 1

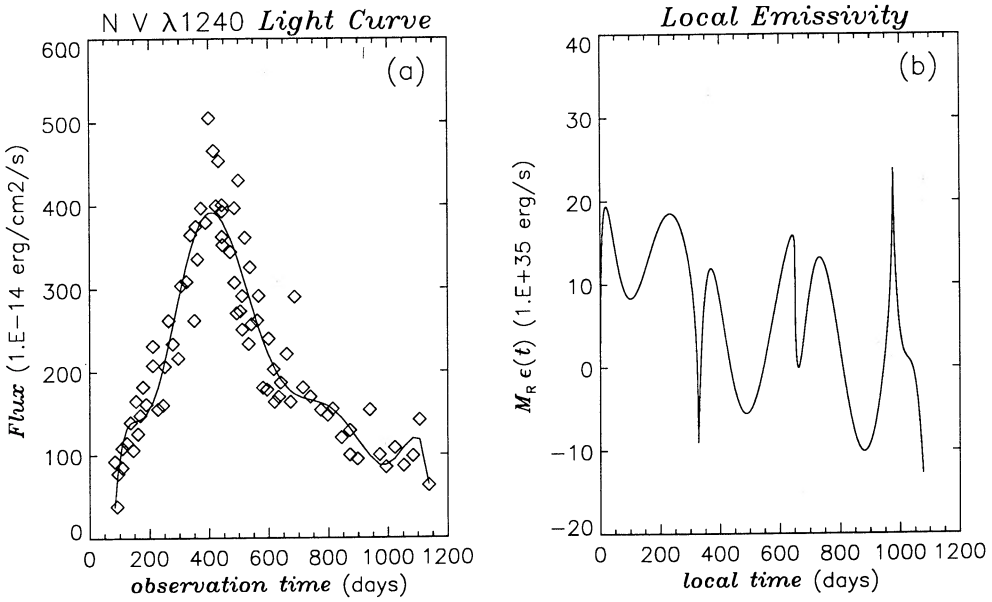

FIG. 8.—Same as Fig. 7, but for the line N V λ1240

$M_\odot$. Therefore their shell becomes highly ionized and optically thin to UV. Nitrogen, for example, is driven into state N VI. We want to distribute roughly the same amount of ionized mass (0.025 $M_\odot$) on a thin ring, keeping ρ the same. Therefore we have to pile it on thickly. If the ring's cross section is roughly circular with diameter $2\pi^{-1/2}A^{1/2}$, then the ring presents a solid angle $4\pi(\pi^{-1/2}A^{1/2}/R)$ to the SN. If $R = 0.65$ lt-yr and $A = 1.8 \times 10^{32}$ cm^2 as above, then the ring occupies only about 1% of the total 4π solid angle. The model UV burst, entering this solid angle, could only ionize $\sim 0.01\ M_\odot$—less than the amount of ionized gas needed in the model. Of course the true UV burst could be stronger (or weaker) than the model burst, and the cross section of ionized mass in the ring need not be circular. The point is that optical thickness effects are likely to be important in a ring model. There may be a Strömgren boundary, with essentially neutral hydrogen on the outer side of the ring. Radiation from N III (for example) may emerge initially from deep layers which were shielded from the full UV blast. Radiation from N V will emerge from shallower layers at the same time. This explains why the best-fit emissivity curves for these two species may be more similar than the corresponding pair computed for the optically thin case by LF.

Suggestive examples of computations for an optically thick ring are given by Lundqvist (1991), but much work remains to be done. Lundquist's (1991) computations give no clue as to why the light curve of the *IUE* line N IV] λ1485 (not shown here) has a different shape, and peaks much earlier ($\approx$320 days; cf. Sonneborn et al. 1990), than those of the N III and N V lines. We would expect the light curve of the N IV line, produced by an intermediate state, to resemble those of the N III and N V lines when the latter two resemble one another.

Surface-brightness observations of the ring in optical lines at several epochs by *HST* will yield information about the emissivity functions $\epsilon(t)$ for those lines. At each epoch, the delay time t is a function of position on the projected ring. However, as pointed out in § 2, the delay times now are all very long. The *IUE* light curves contain information about $\epsilon(t)$ for different lines, and at small values of t, which cannot be obtained from later observations.

Finally we note that continued fluorescence in optical lines such as λ5007 may be due to a region adjacent to the ring "core" with a density lower than the core value ($\sim 10^4$ cm^{-3}) inferred from the *IUE* line emission. Lundqvist (1991) promises further modeling of this. A density gradient could be produced by the progenitor stellar-wind interactions which presumably formed the ring, or by evaporation on the inner side of the ring following the UV burst, so both static and dynamic models must be considered. The surface-brightness observations will give clues about this. Panagia & Gilmozzi (1991) and Panagia et al. (1991) have already proposed a second, lower density component, possibly intermixed with the higher density clouds, to explain the observed patchiness of the ring and the late-time behavior of the UV light curves, along with unpublished observations of the C III] λ1909 doublet.

We thank A. Crotts, C. Fransson, P. Lundqvist, D. E. Osterbrock, N. Panagia, and G. Sonneborn for discussons. This research was supported by NASA Astrophysics Division RTOP 188-44-23-55. J. E. F. thanks the Aspen Center for Physics, where revisions on the manuscript were completed.

REFERENCES

Atherton, P. D., Hicks, T. R., Reay, N. K., Worswick, S. P., & Smith, W. H. 1978, A&A, 66, 297
Bahcall, J. N., Kozlovsky, B.-Z., & Salpeter, E. E. 1972, ApJ, 171, 467
Balick, B., & Preston, H. L. 1987, AJ, 94, 958
Blandford, R. D., & McKee, C. F. 1982, ApJ, 255, 419
Chevalier, R. A. 1986, ApJ, 308, 225
Couderc, P. 1939, Ann. d'Astrophys., 2, 271
Crotts, A. P. S. 1991, in Proc. ESO/EIPC Workshop on Supernova 1987A and Other Supernovae (Marciana Marina, Elba, Italy, 1990 September 17–22), ed. I. J. Danziger & K. Kjär (Garching: ESO), 559
Crotts, A. P. S., & Heathcote, S. 1991, Nature, 350, 683
Crotts, A. P. S., & Kunkel, W. E. 1991, ApJ, 366, L73
Crotts, A. P. S., Kunkel, W. E., & McCarthy, P. J. 1989, ApJ, 347, L61
Curtis, H. D. 1918, Publ. Lick Obs., 13, 55
Dwek, E. 1983, ApJ, 274, 175
Emmering, R. T., & Chevalier, R. A. 1988, AJ, 95, 152
Felten, J. E. 1991, Sky & Telescope, 81, 153
Felten, J. E., & Dwek, E. 1991a, in Proc. ESO/EIPC Workshop on Supernova 1987A and Other Supernovae (Marciana Marina, Elba, Italy, 1990 September 17–22), ed. I. J. Danziger & K. Kjär (Garching: ESO), 569
———. 1991b, BAAS, 23, 972
Felten, J. E., Dwek, E., & Viegas-Aldrovandi, S. M. 1989, ApJ, 340, 943
Fransson, C., Cassatella, A., Gilmozzi, R., Kirshner, R. P., Panagia, N., Sonneborn, G., & Wamsteker, W. 1989, ApJ, 336, 429
Fransson, C., & Lundqvist, P. 1989, ApJ, 341, L59
Girard, T., van Altena, W. F., & Lopez, C. E. 1988, AJ, 95, 58
Heap, S. R., & Lindler, D. J. 1987, A&A, 185, L10
Hinks, A. R. 1902, ApJ, 16, 198
Jakobsen, P., et al. 1991, ApJ, 369, L63
Kapteyn, J. C. 1901, Astron. Nach., 157, 201
Lundqvist, P. 1991, in Proc. ESO/EIPC Workshop on Supernova 1987A and Other Supernovae (Marciana Marina, Elba, Italy, 1990 September 17–22), ed. I. J. Danziger & K. Kjär (Garching: ESO), 607
Lundqvist, P., & Fransson, C. 1991, ApJ, 380, 575 (LF)
Meikle, W. P. S., Cumming, R. J., Spyromilio, J., Allen, D. A., & Mobasher, B. 1991, in Proc. ESO/EIPC Workshop on Supernova 1987A and Other Supernovae (Marciana Marina, Elba, Italy, 1990 September 17–22), ed. I. J. Danziger & K. Kjär (Garching: ESO), 595
Minkowski, R., & Osterbrock, D. E. 1960, ApJ, 131, 537
Morrison, P., & Sartori, L. 1969, ApJ, 158, 541
Morse, P. M., & Feshbach, H. 1953, Methods of Theoretical Physics, Part 1 (New York: McGraw-Hill)
Panagia, N., & Gilmozzi, R. 1991, in Proc. ESO/EIPC Workshop on Supernova 1987A and Other Supernovae (Marciana Marina, Elba, Italy, 1990 September 17–22), ed. I. J. Danziger & K. Kjär (Garching: ESO), 575
Panagia, N., Gilmozzi, R., Macchetto, F., Adorf, H.-M., & Kirshner, R. P. 1991, ApJ, 380, L23
Paresce, F., & Burrows, C. 1989, ApJ, 337, L13
Press, W. H., Flannery, B. P., Teukolsky, S. A., & Vetterling, W. T. 1986, Numerical Recipes: The Art of Scientific Computing (Cambridge: Cambridge Univ. Press)
Reay, N. K., & Worswick, S. P. 1979, A&A, 72, 31
Sonneborn, G. 1989, in 10th Santa Cruz Workshop in Astronomy and Astrophysics (Lick Observatory, 1989 July 9–21), Supernovae, ed. S. E. Woosley (New York: Springer), 125
Sonneborn, G., Cassatella, A., Wamsteker, W., Fransson, C., Kirshner, R., Gilmozzi, R., & Panagia, N. 1990, in Proc. Internat. Symp. on Evolution in Astrophysics (Toulouse, France, 1990 May 29–June 1), ed. E. J. Rolfe (ESA SP-310), 479
Testor, G. 1988, A&A, 190, L1
Walborn, N. R., Lasker, B. M., Laidler, V. G., & Chu, Y.-H. 1987, ApJ, 321, L41
Walker, A. R., & Suntzeff, N. B. 1990, PASP, 102, 131
Wampler, E. J., Wang, L., Baade, D., Banse, K., D'Odorico, S., Gouiffes, C., & Tarenghi, M. 1990, ApJ, 362, L13
Wood, P. R., & Faulkner, D. J. 1989, IAU Circ., No. 4739
Wright, E. L. 1980, ApJ, 242, L23